Journal of Saudi Chemical Society (2023) 27, 101713

King Saud University

Journal of Saudi Chemical Society

www.ksu.edu.sa
www.sciencedirect.com

ORIGINAL ARTICLE

Non-cytotoxic and bioactive nanocomposite film of natural Arabic gum incorporating TiO_2 nanoparticles for bone tissue regeneration

Xinyu Fan [a], Weiwei Wang [b], Nan Jiang [a], Baochuang Qi [a], Gang Li [a], Zhuo Peng [a], Yin Yang [a], Yongqing Xu [a,*], Mahani Yusoff [c], Mohd Hasmizam Razali [d,e]

[a] *Department of Orthopaedics, 920th Hospital of the Joint Logistics Support Force of the PLA, Kunming 655000, China*
[b] *Department of Chest Surgery, The Third Affiliated Hospital of Kunming Medical University (Tumor Hospital of Yunnan Province), Kunming, Yunnan 655000, China*
[c] *Faculty of Bioengineering and Technology, Universiti Malaysia Kelantan, 17600 Jeli, Kelantan, Malaysia*
[d] *Faculty of Science and Marine Environment, Universiti Malaysia Terengganu, 21030 Kuala Nerus, Terengganunu, Malaysia*
[e] *Advanced Nanomaterials Research Group, Faculty of Science and Marine Environment, Universiti Malaysia Terengganu, 21030 Kuala Nerus, Terengganunu, Malaysia*

Received 19 June 2023; revised 26 July 2023; accepted 7 August 2023
Available online 14 August 2023

KEYWORDS

Nanocomposite;
Film;
Gum;
TiO_2;
Nanoparticle;
Bone tissue

Abstract Biomaterials with exceptional biocompatibility and bioactivity are now pushing the boundaries of bone tissue engineering. In this study, natural Arabic gum biopolymer incorporating titanium dioxide nanoparticles (NAG + TiO_2NP) nanocomposite film was fabricated. The FTIR and XRD analysis show the presence of functional groups assigned to NAG biopolymers and highly crystalline anatase TiO_2NP. Well dispersed TiO_2NP can be seen from SEM micrograph suggesting good interaction between TiO_2NP filler and NAG biopolymer matrix to enhance the mechanical characteristics of nanocomposite film. The NAG + TiO_2NP nanocomposite film exhibited strong bioactivity to form bone-like apatite and promoted the proliferation of MG-63 cells attributed to their excellent biocompatibility and non-toxicity. The NAG + TiO_2NP nanocomposite film also displays high antibacterial activity with (36.33 ± 1.53) mm and (27.00 ± 2.00) mm inhibition zone were recorded against *Staphylococcus aureus* and *Escherichia coli*. The findings indicate that the NAG + TiO_2NP nanocomposite film, with its improved mechanical properties, high swelling capacity, biodegradability, and non-toxicity, shows promise as a viable option for bone tissue regeneration materials.

* Department of Orthopaedics, 920th Hospital of the Joint Logistics Support Force of the PLA, Kunming 650000, China (Y. Xu).
E-mail addresses: dr_xyq774655@sina.com (Y. Xu), mdhasmizam@umt.edu.my (M.H. Razali).

https://doi.org/10.1016/j.jscs.2023.101713
1319-6103 © 2023 The Author(s). Published by Elsevier B.V. on behalf of King Saud University.

1. Introduction

Physically and functionally, bone is a very dynamic and varied tissue in the human body. Long to short, flat, and crooked bones make up the human skeletal structure. Bone pores typically range in size from 100 to 300 μm. Nutritional active diffusion takes place 150–200 μm pore diameters away from the blood supply. The primary components of bone extracellular matrix are nonmineralized and mineralized phases [1]. The nonmineralized phase is typically a biopolymer that encompasses glycoprotein, proteoglycans, glycosaminoglycans, and type-I collagen, while the mineralized phase primarily consists of $Ca_{10}(PO_4)_6(OH)_2$ hydroxyapatite (HAp) [2]. Currently, bone grafts or synthetic materials are utilized to regenerate bone tissue; however, these methods are hindered by limitations such as restricted availability, donor site morbidity, immune rejection, and suboptimal integration with host tissue [3]. Hence, there is a requirement to explore innovative approaches, such as tissue engineering, biomaterials, and cellular therapies, to surmount these obstacles and augment the regenerative capacity of bone tissue.

Biopolymers are widely utilised in bone tissue regeneration because they are flexible, lightweight, and simple to manufacture biomedical materials. Degradable biopolymers including collagen, hyaluronan, chitosan, gelatin, alginate, and gum that are found in nature are used to create scaffold materials. However, biopolymers cannot solely accomplish the requirements of an ideal biomaterial, necessitating the incorporation of inorganic reinforcements. In a bioactive composite, the biopolymers as a matrix and the fillers serve as reinforcement [4,5]. The combination of polymeric components and reinforcements increased the mechanical strength of composite materials. On top of that, the physical and chemical characteristics of the manufactured composite materials was varied. Recent research has demonstrated the superior biocompatibility and osteogenic qualities of bioactive nanocomposites, as well as high mechanical strength (to support structures) for biomedical application [6,7]. As a result, the biopolymeric bioactive nanocomposites were extensively studied.

Arabic gum (AG) biopolymer is a complex mixture of polysaccharides, their salts (calcium, magnesium, and potassium), and glycoproteins that is collected as a dried exudate from the stems and branches of acacia trees. L-arabinose, D-galactose, rhamnose, and glucuronic acid were produced by the hydrolysis of AG [8]. The present study has selected natural Arabic gum (NAG) as the biopolymer matrix, due to its noteworthy properties such as water solubility, absence of toxicity, and a straightforward extraction method [8]. The NAG was incorporated with titanium dioxide nanoparticles (TiO_2 NP) to promote the bio-compatibility and bioactivity of the nanocomposite for bone tissue regeneration. According to the Food and Drug Administration (FDA), titanium dioxide (TiO_2) is one of the most biocompatible and hydrophilic inorganic nanoparticles and is thought to be non-toxic, environmentally friendly, and biosafe. The nano TiO_2 surface's abundant hydroxyl (—OH) groups allow for the functionalization and grafting of organic and biopolymer chains [9]. Moreover, the nature of the biopolymer and nanoparticles, as well as their molecular size, shape, surface charge density, polymer-particle affinity, interactions, and ratio, substantially influenced their functional features.

As noted in previous research, Fourier Transform Infrared (FTIR) confirmed the feasibility of natural biopolymer-TiO_2 interactions [10,11]. For example, sage seed gum (SSG) chains contain a number of carboxyl and hydroxyl agents, giving TiO_2NP surface a lot of potential binding sites as TiO_2 has a great affinity for carboxyl (—COOH) groups. Additionally, the Ti atoms on the nano-TiO_2 can be coordinated by carboxylate groups on the repeating units of SSG chains in three separate unidentate, chelating, and bridge bidentate modes [12]. The presence of hydrogen bonding, or H-bonding, as a crucial interaction in the SSG-TiO_2 hybrid composite is highly anticipated, as it contributes significantly to the enhancement of mechanical properties. These benefits render TiO_2NP an optimal inorganic strengthening element in the production of SSG-based nanohybrid hydrogel with novel and promising functional properties and applications.

Incorporating nano-sized materials offers significant advantages in reducing the surface area-to-volume ratio [13], owing to their larger surface area compared to their bulk counterparts. This increased surface area allows for more interactions with surrounding biological tissues and cells [14]. In the context of bone tissue regeneration, nanomaterials provide a larger contact area for cell adhesion, proliferation, and differentiation, facilitating faster and more efficient bone formation [15]. Nanomaterials also exhibit improved biocompatibility due to their resemblance to the natural components of bone tissue at the molecular level. This helps in reducing adverse reactions and immune responses, making them more suitable for implantation and integration with the host tissue to promote the cells growth and differentiation [16]. Nanomaterials have gained significant attention as a remarkable class of materials due to their unique properties and the fact that they encompass a wide range of samples with at least one dimension ranging from 1 to 100 nm [17]. It is worth noting that nanomaterials can stimulate the expression of certain human genes involved in bone growth and repair, those encoding for growth factors and extracellular matrix proteins [18]. Notably, TiO_2 nanomaterials have been incorporated into various forms of biopolymer matrices, such as film, fluid, and double-network gel. In particular, the incorporation of TiO_2-NP into biopolymers has shown substantial potential in overcoming these obstacles by providing enhanced biocompatibility, mechanical properties, and osteo-inductive properties. The nanoparticles also play an important role in speeding recovery and reducing toxic side effects [19]. Nonetheless, it remains imperative to address key research questions and optimize the incorporation process. These questions include evaluating the biocompatibility and cytotoxicity of the TiO_2NP incorporated biopolymers, assessing the in vivo performance and biodegradability of the nanocomposite film, investigating the impact on mineralization of bone-forming cells. Ultimately, the aim is to develop TiO_2NP incorporated NAG biopolymers as a safe and effective biomaterial for bone tissue regeneration.

2. Experimental

2.1. Chemical

Natural Arabic gum (NAG) powder is a Sudan product branded ALNOOR. Titanium dioxide nanoparticles (TiO_2NP)

(anatase, Mw 79.87 g/mol, product number 13463-67-7, lot number K45324808505), and calcium chloride ($CaCl_2$) (CAS number 10043-52-4, lot number K47117278604) were obtained from Merck, Malaysia. Glycerol (product number G5516, lot number STBC1888V) obtained from Sigma-Aldrich, Malaysia. All materials were used as received.

2.2. Preparation

A solution of NAG was produced through the dissolution of 10 g of NAG in 100 mL of deionized water, while maintaining continuous stirring for a duration of two hours at a temperature of 70 °C. To this solution, 0.5 g of glycerol (5 w/w%, relative to NAG) and 5 mL $CaCl_2$ (at a concentration of 5 mM) were subsequently added. Following this, 0.1 g of TiO_2NP (1 w/w% relative to NAG) was added to the solution while stirring for an additional two hours and sonication with 24 kHz Hielscher UP200H ultrasound (Hielscher Ultrasonics, Germany) for 5 min at ambient temperature. The resulting solution was then transferred to a casting dish, where it was dried in an oven for a period of 24 h at a temperature of 50 °C, thus producing a film. All films were preconditioned in a desiccator, at a temperature of 27 °C and relative humidity of 50%, for a minimum of two days prior to testing. A pure NAG film was fabricated using a procedure similar to the one described earlier, however, in the absence of TiO_2 nanoparticles. Prior to the generation of the film, an optimization study was conducted to determine the ideal concentration of materials required to produce a film of high quality [20].

2.3. Characterization

The presence of bands corresponding to various functional groups in the nanocomposite films had been studied using FTIR spectra in the range 4000–400 cm^{-1} with a resolution of 4 cm^{-1} at room temperature on a Perkin Elmer 2400 as a preliminary investigation regarding chemical interactions between various components. X-ray diffractometer (XRD) was utilised to analyse the film samples' crystallinity and phase transitions. The results were collected using a Bruker AXS D8 Advance XRD, operating at 40 kV, 30 mA, with Cu K radiation (1.540 A) at a 2° angle between 10° and 70°. The surface morphology of nanocomposite films was shown by SEM image from a scanning electron microscope (SEM JEOL, Japan). The samples were operated at a voltage of 15 kV and had gold particles applied to them.

The mechanical properties of films were studied utilizing the Instron Universal Testing machine (model 3366) in accordance with the ASTM D882 [21] standard. To accomplish this, rectangular strips measuring 2.0 × 6.0 cm were dissected from the specimens, and five specimens of each sample were subjected to testing.

The process of measuring the swelling properties involved the weighing of dried films (W_{dry}) followed by immersion into 50 mL phosphate buffer saline (PBS) (Sigma-Aldrich, Malaysia) of pH 7 at 37 ± 0.5 °C. After 24 h, the films were weighed again (W_{wet}) and the degree of swelling (%) was determined using the following equation (1):

$$\text{Swelling } (\%) = \frac{(W_{wet} - W_{dry})}{W_{dry}} \times 100 \quad (1)$$

where W_{dry} and W_{wet} represent the initial weight and final weight of the films, respectively. It is noteworthy that a minimum of five independent measurements were conducted per sample.

The assessment of the biodegradation of pure NAG film and NAG + TiO_2NP nanocomposite film was conducted through incubation at a temperature of 37 °C in PBS. The films were cut into identical sizes, and their initial weight prior to immersion in PBS was denoted as W_i. After a specified duration, the film was removed, washed with DI water, dried, and weighed again, with the resulting weight being noted as W_f. To determine the rate of film degradation, Eq. (2) was employed;

$$\text{Degradationrate } (\%) = \frac{(W_i - W_f)}{W_i} \times 100 \quad (2)$$

2.4. Antibacterial study

In this research, an anti-bacterial assay was conducted utilizing Gram-positive (*Staphylococcus aureus*) and Gram-negative (*Escherichia coli*) microbes. The standard growth medium employed was the Muller-Hinton (MH) agar (Sigma-Aldrich, Malaysia), which was prepared by sterilization with an autoclave for 15 min at 120 °C. Prior to bacterial inoculation, both *Staphylococcus aureus* and *Escherichia coli* strains were subcultured in MH agar and subsequently incubated aerobically at 37 °C for 24 h to ensure a stable bacterial condition devoid of any contamination. To determine bacterial concentrations, a simple optical density measurement was conducted via a Spectrophotometer Biomerieux Densicheck Plus at 600 nm. Equivalence of turbidity at 0.5 McFarland standards was achieved for all bacterial suspensions in this study. In sterile Petri plates containing the MH agar, inoculants of *Staphylococcus aureus* and *Escherichia coli* were evenly spread. A sterile cotton swab was employed to swab all bacteria over the surface of the agar plates. The films sample and penicillin as a control were gently pressed on the agar.

2.5. Cytotoxicity study

The cytotoxicity of the films and its impact on cell viability were evaluated through cell proliferation analysis using (3-(4, 5-dimethylthiazol-2-yl)-2,5-diphenyltetrazolium bromide) (MTT) (Thermo Fisher Scientific, USA) assays, which was conducted in accordance with the ISO 10993-5 test protocol. In this assay, human osteosarcoma (MG-63) cells were initially seeded in 96-well cell culture plates at a density of 5000 cells per well. Subsequently, the specimen was introduced to the cells and incubated for a duration of 24 and 48 h within an incubator containing 5% CO_2 at 37 °C. After 24 and 48 h of incubation, 50 µl of the MTT test solution was administered to each plate, and the cell culture plates were then placed inside the incubator and incubated at 45 °C for 60 min. Untreated cells were designated as control cells and deemed to have complete viability, whereas the viability of treated cells was denoted as a percentage in comparison to the control cells. The measurements were performed thrice using the ELISA Reader (Tecan, Switzerland) within the reference wavelength range of 460–520 nm.

2.6. Bioactivity study

Using a simulated bodily fluid (SBF) solution, which has nearly identical ion concentration as human blood plasma, the bioactivity of NAG + TiO_2NP nanocomposite film was studied. The SBF solution was prepared following the method previously described in Ref. [22]. The NAG + TiO_2NP nanocomposite film, all of equal dimensions, were immersed in the SBF solution and were subjected to a culture period of seven days at a temperature of 37 °C. After a week of incubation, SEM, FTIR and XRD analysis were performed on the samples to evaluate their ability to generate apatite.

3. Results and discussion

Fig. 1 depicts the tangible manifestations of natural Arabic gum (NAG) film and natural Arabic gum incorporating titanium dioxide nanoparticles (NAG + TiO_2NP) nanocomposite film. The dimensions of the films, in terms of both diameter and thickness were observed to be approximately ~9 cm and ~65 μm, respectively.

The FTIR spectra of the pure NAG and NAG + TiO_2NP nanocomposite films were shown in Fig. 2. Through FTIR spectral analysis, it was feasible to discern the distinctive traits of the precursor materials within the film composition. The band located at 3300 cm^{-1} signifies the elongation vibration of the —OH groups that are present in the chemical composition of pure NAG film and NAG + TiO_2NP nanocomposite film. Additionally, a discrete band was observed at 1605 cm^{-1}, which emanated from the deformation of the OH groups [23]. The stretching vibration of C—H groups from the biopolymer carbon chains is represented by the discreet band located at 2922 cm^{-1} [23]. The band obtained at 2362 cm^{-1} results from stretching modes of the carboxylic acid group and the presence of the band at 1740 cm^{-1} because of C═O stretching [24]. Two strong bands at 1417 cm^{-1} and 1370 cm^{-1} were due to C═O symmetric and asymmetric stretching vibration [25]. While, the band at 1224 cm^{-1} was appeared because of C—O—C stretching vibration indicating the glycosidic bonds present in both samples [26]. Lastly, the presence of a characteristic peak positioned at approximately 1017 cm^{-1} corresponds to the alkene C—H bending in polysaccharides natural Arabic gum specimens [27]. A distinct peak at 429 cm^{-1} was only detected in the NAG + TiO_2NP nanocomposite film sample specifically related to metal oxide bonding [28]. This occurrence can be attributed to the Ti-O bond, therefore signifying the triumphant integration of TiO_2NP into NAG.

Fig. 3 presents the X-ray diffraction (XRD) patterns of pure NAG film and NAG + TiO_2NP nanocomposite film. For pure NAG film, a board peak at $2\theta = 21.12°$ was observed which is corresponds to the lattice plane (1 1 0) and indicates that the NAG sample is in amorphous state. This observation is consistent with previous researchers who have noted that the amorphous nature of gum [25,26]. Upon the incorporation of TiO_2NP, similar broad peak was observed at 19.92°, slightly lower as compared to pure NAG with low intensity indicating the interaction between NAG biopolymer matrix and TiO_2NP filler. Nevertheless, high intensity peaks were observed at 2θ of 25.74°, 38.40°, 48.46°, 54.46°, 55.54°, 63.23°, 69.28°, 70.86°, and 75.60°, which is refer to the anatase TiO_2 phase, suggesting that highly crystalline of TiO_2NP was successfully loaded onto the NAG + TiO_2NP nanocomposite film as supported by SEM image.

The SEM image in Fig. 4(a), displays a crack rough surface indicating low mechanical property of the pure NAG film. In contrast, the inspection of the SEM image revealed no evidence of cracking, splitting, or cleavages in the NAG + TiO_2-NP nanocomposite film (Fig. 4(b), suggesting that the lower air permeability led to a stronger core material loading of the nanocomposite. These results may be attributed to the formation of intermolecular hydrogen bonding between biopolymer and TiO_2NP [29–31]. The conspicuous existence of TiO_2NP can be seen in the SEM image, exhibiting a well-distributed and near-spherical configuration. These observations suggest that TiO_2NP and NAG have established a strong interconnection, leading to the formation of a high-quality nanocomposite material.

Table 1 presents the mechanical characteristics of prepared films. The results indicate that the inclusion of TiO_2NP is beneficial for enhancing the strength of nanocomposite films, as evidenced by the increase in young modulus (YM) and tensile strength (TS) from 44.41 ± 2.93 to 75.22 ± 3.48 and 2.44 ± 1.18 MPa to 4.86 ± 1.22 MPa, respectively. This improvement is attributed to the uniform dispersion of TiO_2NP filler within the matrices of NAG indicating a favourable interfacial interaction between TiO_2NP and NAG [32]. The Young's modulus

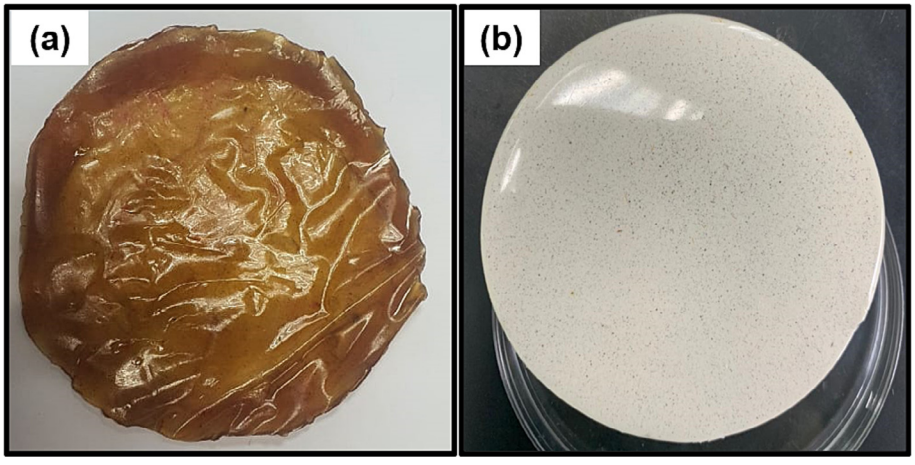

Fig. 1 Physical appearance of (a) pure NAG film and (b) NAG + TiO_2NP nanocomposite film.

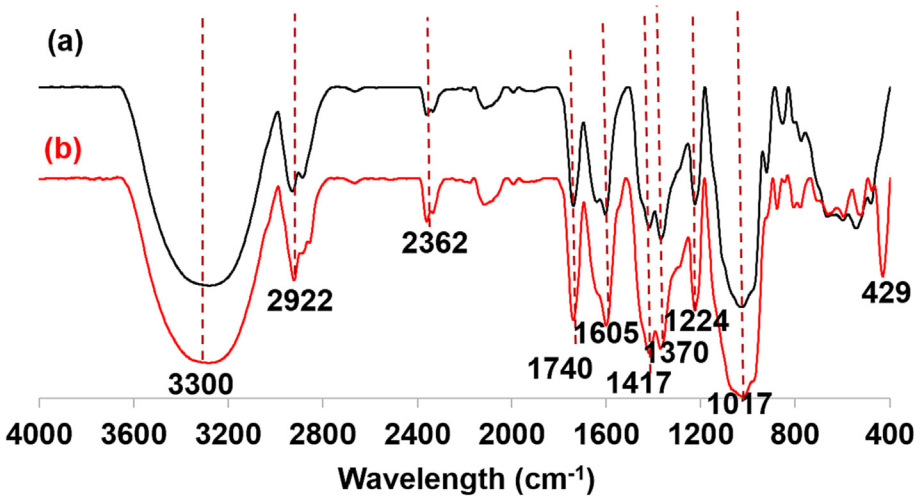

Fig. 2 FTIR spectra (a) pure NAG film and (b) NAG + TiO_2NP nanocomposite film.

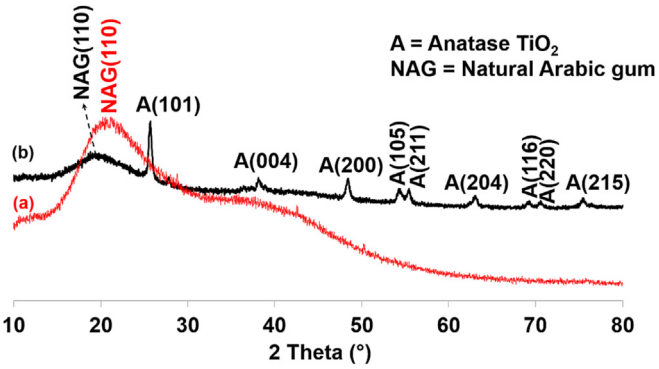

Fig. 3 XRD patterns of (a) pure NAG film and (b) NAG + TiO_2NP nanocomposite film.

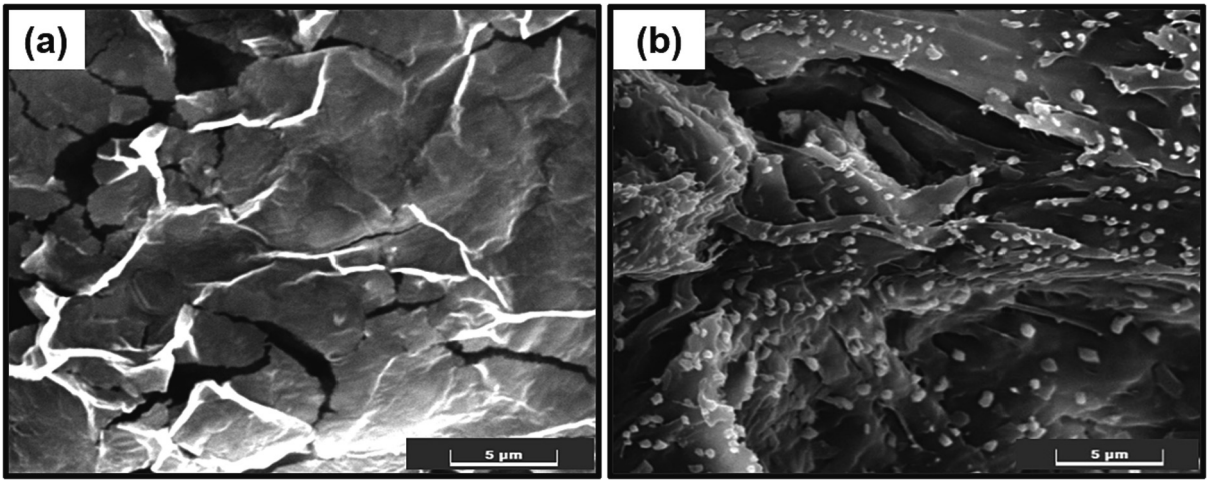

Fig. 4 SEM micrographs of (a) pure NAG film and (b) NAG + TiO_2NP nanocomposite films.

of NAG + TiO_2NP nanocomposites film nanocomposites was enhanced as compared to pure NAG film. This increase in stiffness can be attributed to the high crystallinity nature of TiO_2NP. However, the presence of TiO_2NP in the NAG film resulted in a significant decrease in elongation at break (EAB). This phenomenon suggests that the segment movement of NAG matrices was restricted during stretching.

The efficient absorption rate of biological fluids in the surrounding area of the implanted film is a crucial factor for consideration. The assessment of swelling behaviour of films are therefore of utmost importance. In this regard, the NAG + TiO_2NP nanocomposite film exhibited greater swelling percentages with 1280 ± 8%, as compared to 940 ± 6% for pure NAG film, which is conducive to the adhe-

Table 1 Thickness, mechanical properties, and swelling of NAG and NAG + TiO_2-NP nanocomposite film.

Sample	Thick (μm)	TS (MPa)	YM (MPa)	EAB (%)	Swelling (%)
NAG	65.04 ± 0.22	2.44 ± 1.18	44.41 ± 2.93	10.61 ± 0.48	940 ± 6
NAG + TiO_2NP	65.08 ± 0.18	4.86 ± 1.22	75.22 ± 3.48	8.81 ± 0.62	1280 ± 8

(mean ± SD) (n = 5); TS (tensile strength), YM (Young's modulus), EAB (elongation-at-break).

sion and proliferation of cells on the films. A higher swelling index can also facilitate the transportation of nutrients and fluid uptake from the medium [33]. The hydrophilic nature of NAG may be attributed to the enhanced swelling behaviour of the NAG + TiO_2NP nanocomposites film [34].

Biodegradability constitutes an essential characteristic of biomaterial, whereby the films must degrade simultaneously with the complete regeneration of the films' functional site. To assess biodegradability, the biodegradation test was conducted in PBS at body temperature for a duration of three weeks. On day seven, the biodegradation rate of NAG + TiO_2-NP nanocomposite film was shown to be comparable to that of pure NAG which are 22% and 20%, respectively. While on days 14 and 21, the biodegradation rate of NAG + TiO_2NP nanocomposite film was increased more rapidly to 56% and 88% as compared to 38% and 64% for pure NAG film, which may be attributed to the possible interaction of TiO_2NP with the NAG matrix. The results obtained from the swelling and degradation behaviour analysis were found to be interrelated. Matrices with higher swell ability interact with a greater number of H_2O molecules, resulting in the quicker degradation of films. Conversely, slowly degrading matrices exhibited lower swelling ratios [35]. However, the films are expected to dissolve in the body without posing any accumulation or hazardous effects.

The present study employed the disc diffusion method to explore the antibacterial activity of biofilms against gram-positive (*Staphylococcus aureus*) and gram-negative (*Escherichia coli*) bacterial strains. The occurrence of clear inhibition zones around the discs was indicative of a positive antibacterial result, and the activity was quantified by measuring the diameter of the clear zone of inhibition as illustrated in Fig. 5. The antibacterial results presented in Table 2, was compared to those of the standard drug, penicillin and revealed that NAG + TiO_2NP nanocomposite film exhibited superior antibacterial activity against *Staphylococcus aureus* and *Escherichia coli*. The enhanced efficacy of NAG + TiO_2NP nanocomposite film can be attributed to the coulombic attraction that facilitates the interaction between micro-organisms carrying a negative charge and the net positive charge of the metal oxide, TiO_2 [36,37]. It has been previously reported that the incorporation of nanoparticles into polymer nanocomposites leads to improved antibacterial activity due to the presence of TiO_2, which can induce deformities in bacterial cell walls, thereby rendering them leaky and ultimately resulting in bacterial death [38–40].

Table 2 Inhibition zone of films and penicillin against *Staphylococcus aureus* and *Escherichia coli*.

Diameter of Inhibition (mm)		
Sample	*Staphylococcus aureus*	*Escherichia coli*
Penicillin	17.67 ± 0.58	12.33 ± 1.53
NAG	–	–
NAG + TiO_2NP	36.33 ± 1.53	27.00 ± 2.00

(mean ± SD) (n = 3).

The present study conducted the in-vitro cytotoxicity of both prepared films against the human osteosarcoma cell line (MG-63) through MTT assay. The experiment involved treating the films' surface with MG-63 cells for 24 and 48 h, respectively, to detect cell proliferation and viability. The results demonstrated that the incorporation of TiO_2NP into the films did not have any adverse effects on the viability of cells. In fact, the NAG + TiO_2NP nanocomposite films' surface exhibited better cell proliferation compared to the control group. The nanocomposite films' cell viability also showed an increase to 120.73% after 24 h and 144.12% after 48 h, as compared to the control group. Pure NAG film also shows an increased in the number of cells after 24 h and 48 h, respectively. Therefore, it can be inferred that the viability of cell towards both films improved with an increase in culturing time and that the addition of TiO_2NP did not have any cytotoxic effects on the film. The hydrophilic nature of the NGA biopolymer material in the nanocomposite demonstrates excellent biocompatibility and facilitates cell-material interaction [41]. Moreover, TiO_2NP was reported non-toxic in nature [42,43], hence, it can be concluded that NAG + TiO_2NP nanocomposite film is capable of promoting good growth and proliferation of MG-63 cells.

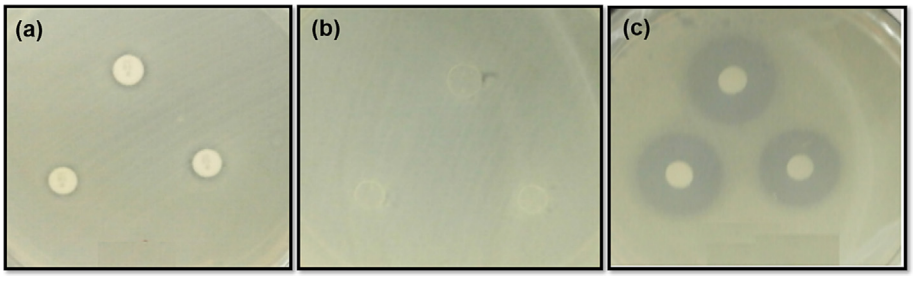

Fig. 5 Photographs of antibacterial test result of (a) penicillin, (b) pure NAG film and (c) NAG + TiO_2NP nanocomposite against *Staphylococcus aureus* bacteria.

Bioactivity, a significant property of biomaterials, pertains to the capacity to generate a mineralized apatite layer on the surface of a material in the SBF [22]. Following immersion in the SBF solution for a period of 7 days, the apatite layer formed on the surface was analysed by SEM, FTIR, and XRD. After immersion, the presence of double peaks at 556 cm^{-1} and 596 cm^{-1} were observed in the FTIR spectrum (Fig. 6(a), corresponds to the bending mode of orthophosphate and lends support to the formation of HA. According to the previous researchers, the primary peaks utilized for characterizing the HA layer are two P-O bending peaks with a frequency at ~560 and ~603 cm^{-1} [44,45]. Moreover, the presence of strong band at 1022 cm^{-1} represents the PO_4^{3-} group's vibrations [46,47], suggesting that the formation of hydroxyapatite (HA) was in the crystalline phase on the surface of nanocomposite film. Moreover, the X-ray diffraction (XRD) in Fig. 6b, exhibiting high intensity and sharp peaks at 2θ of 21.54°, 22.45°, 31.62°, 32.06°, 40.61°, 45.32°, and 56.38°, thus verifying the high degree of crystallinity of the specimen. The highest intensity of peak situated at 31.62° assigned to the crystal planes denoted by Miller indices (2 1 1) of HA [48,49]. Thus, the XRD result this finding reveals the formation of the HA layer and consistent with the FTIR results obtained in this study.

Moreover, the SEM image in Fig. 7(a), shows the formation of the HA apatite layer in comparison to SEM images before immersion. Evidently, the surface was rough, with numerous apatite cluster accumulating on the surface, consistent with a similar investigation [50]. In order to determine the molar ratio of the Ca/P, the EDS analysis was also performed

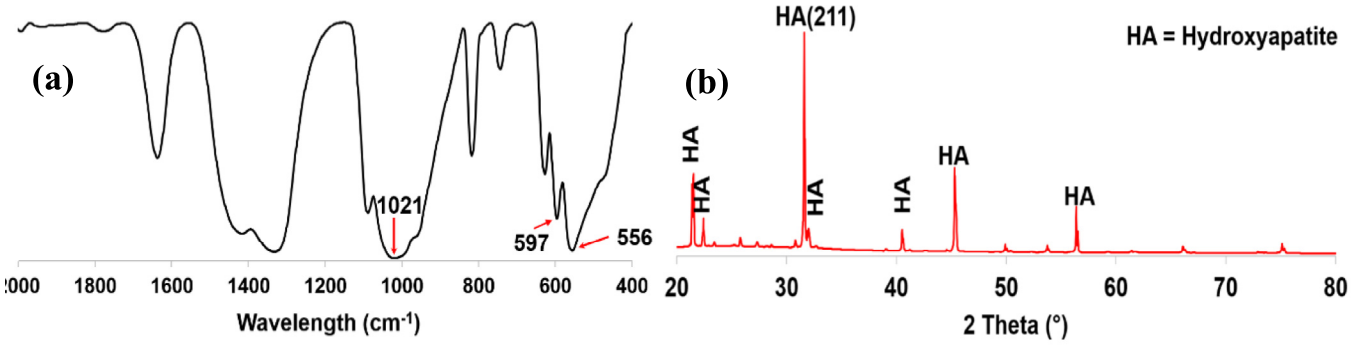

Fig. 6 (a) FTIR spectra and (b) XRD pattern of NAG + TiO_2NP nanocomposite film after immersion in SBF for 7 days.

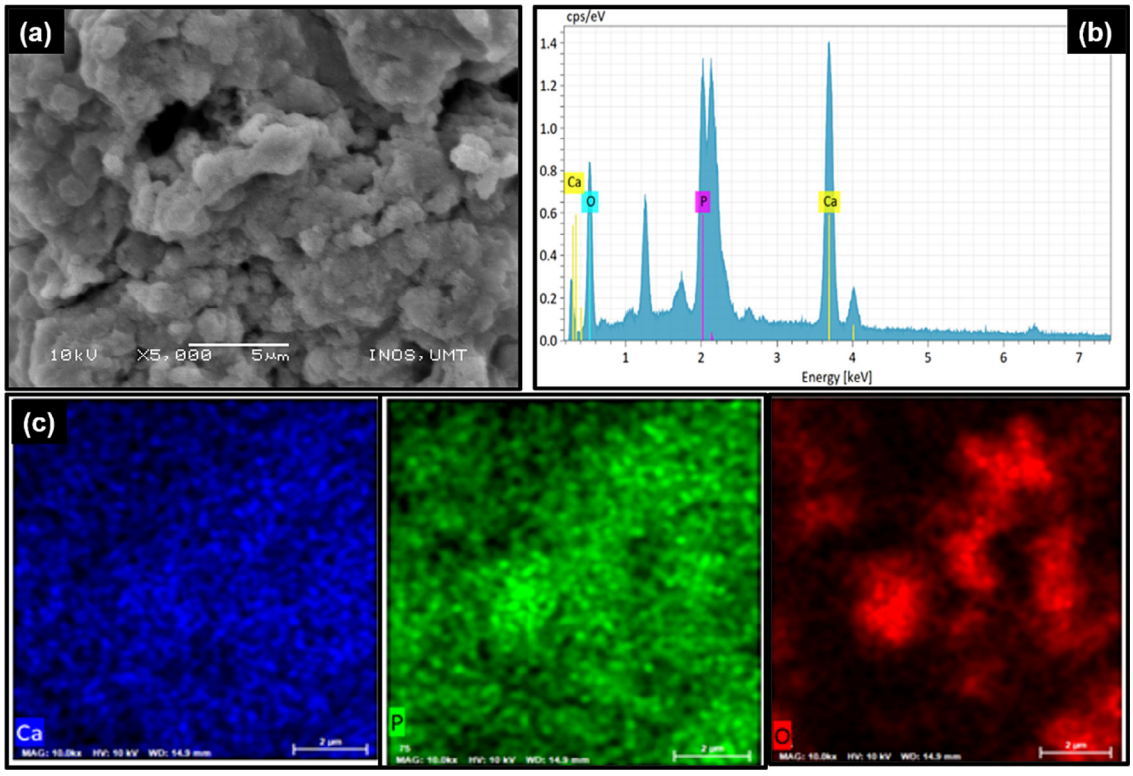

Fig. 7 (a) SEM image, (b) EDX spectrum and (c) elemental mapping images of Ca, P and O on NAG + TiO_2NP nanocomposite film after immersion in SBF for 7 days.

on the surface of the nanocomposite film as shown in Fig. 7(b). Fig. 7(c) shows the elemental mapping of Ca, P as well as O which are corresponding to the chemical formula of HA, $Ca_{10}(PO_4)_6OH_2$. The EDS data confirmed that Ca and P elements dominated the precipitated layers on the surface. In addition, the Ca and P ratios was found to be 2.89, which is higher than that of HA in natural bone (1.86) [51], indicating a marginally more rapid formation rate of HA on NAG + TiO_2NP nanocomposite film. In contrast, the pristine TiO_2NP powder sample did not exhibit the presence of HA after being immersed in SBF for 21 days [52]. This could be attributed to the particles settling at the tube's bottom, offering limited surface area for HA nucleation [52]. Additionally, at the nanoscale, pristine TiO_2NPs tend to agglomerate, potentially leading to cytotoxicity [53].

4. Conclusion

The present study successfully fabricated the NAG + TiO_2NP nanocomposite film using solvent casting method with desirable structures, high swelling and improved mechanical properties. Incorporating the TiO_2NP fillers into the NAG matric biopolymer enhanced the biological features thereby improving its bioactivity. The highly bioactive nature of the NAG + TiO_2NP nanocomposite film was confirmed by the formation of HA on the film after immersion in SBF, as shown by the results of SEM and EDX analysis. The antibacterial activity of the NAG + TiO_2NP nanocomposite film against gram positive and gram negative strains can be attributed to the presence of TiO_2NP. The biocompatibility test revealed that the NAG + TiO_2NP nanocomposite film promoted cell proliferation, indicating its non-toxicity. These results support the potential use of the NAG + TiO_2NP nanocomposite film as a viable bioactive material for bone tissue regeneration.

Funding

Grants from Yunnan Orthopedics and Sports Rehabilitation Clinical Medicine Research Center (No. 202102AA310068). Yunnan Prvincial Clinical Orthopaedic Trauma Medical Center (No. ZX20191001). Clinical Key Subject Construction Project of PLA. Medical key subject of Joint Logistics Support Force of PL References.

Declaration of Competing Interest

The authors declare that they have no known competing financial interests or personal relationships that could have appeared to influence the work reported in this paper.

References

[1] D. Logeart-Avramoglou, F. Anagnostou, R. Bizios, H. Petite, Engineering bone: challenges and obstacles, J. Cell Mol. Med. 9 (1) (2005) 72–84.
[2] M.U.A. Khan, S. Haider, S.A. Shah, S.I. Abd Razak, S.A. Hassan, M.R.A. Kadir, A. Haider, Arabinoxylan-co-AA/HAp/TiO_2 nanocomposite scaffold a potential material for bone tissue engineering: An in vitro study, Int. J. Biol. Macromol. 151 (2020) 584–594.
[3] H. Chen, R. Truckenmüller, C. Van Blitterswijk, L. Moroni, Fabrication of nanofibrous scaffolds for tissue engineering applications, in: A.K. Gaharwar, S. Sant, M.J. Hancock, S.A. Hacking (Eds.), Nanomaterials in Tissue Engineering, Woodhead Publishing, Netherlands, 2013, pp. 158–183.
[4] B.K. Shanmugam, S. Rangaraj, K. Subramani, S. Srinivasan, W.K. Aicher, R. Venkatachalam, Biomimetic TiO_2-chitosan/sodium alginate blended nanocomposite scaffolds for tissue engineering applications, Mater. Sci. Eng. C 110 (2020) 110710.
[5] P. Ezati, S. Roy, J.W. Rhim, Pectin/gelatin-based bioactive composite films reinforced with sulfur functionalized carbon dots, Colloids Surf. A Physicochem. Eng. Asp. 636 (2022) 128123.
[6] S.M. Mousavi, S.A. Hashemi, M.Y. Kalashgrani, N. Omidifar, S. Bahrani, N. Vijayakameswara Rao, A. Babapoor, A. Gholami, W.H. Chiang, Bioactive graphene quantum dots based polymer composite for biomedical applications, Polymers 14 (3) (2022) 617.
[7] Z. Guo, A.A. Poot, D.W. Grijpma, Advanced polymer-based composites and structures for biomedical applications, Eur. Polym. J. 149 (2021) 110388.
[8] J. Defaye, E. Wong, Structural studies of gum arabic, the exudate polysaccharide from Acacia senegal, Carbohydr. Res. 150 (1) (1986) 221–231.
[9] A.M. Mariana, L.B. María, V. Lorena, D.B. Claudio, Gum arabic: More than an edible emulsifier, products and applications of biopolymers, in: C.J.R. Verbeek (Ed.), Products and Application of Biopolymer, In Tech PublishIng, Switzerland, 2012, pp. 3–26.
[10] S.L. Young, X. Sarda, M. Rosenberg, Microencapsulating properties of whey proteins. 2. Combination of whey proteins with carbohydrates, J. Dairy Sci. 76 (10) (1993) 2878–2885.
[11] S.A. Oleyaei, H. Almasi, B. Ghanbarzadeh, A.A. Moayedi, Synergistic reinforcing effect of TiO_2 and montmorillonite on potato starch nanocomposite films: thermal, mechanical and barrier properties, Carbohydr. Polym. 152 (2016) 253–262.
[12] S.A. Oleyaei, Y. Zahedi, B. Ghanbarzadeh, A.A. Moayedi, Modification of physicochemical and thermal properties of starch films by incorporation of TiO_2 nanoparticles, Int. J. Biol. Macromol. 89 (2016) 256–264.
[13] N. Hossain, M.H. Mobarak, A. Hossain, F. Khan, J.J. Mim, M. A. Chowdhury, Advances of plant and biomass extracted zirconium nanoparticles in dental implant application, Heliyon (2023) 1–12.
[14] A.E. Nel, L. Mädler, D. Velegol, T. Xia, E.M. Hoek, P. Somasundaran, F. Klaessig, V. Castranova, M. Thompson, Understanding biophysicochemical interactions at the nano–bio interface, Nat. Mater. 8 (7) (2009) 543–557.
[15] S. Duan, X. Yang, F. Mei, Y. Tang, X. Li, Y. Shi, J. Mao, H. Zhang, Q. Cai, Enhanced osteogenic differentiation of mesenchymal stem cells on poly (l-lactide) nanofibrous scaffolds containing carbon nanomaterials, J. Biomed. Mater. Res. A 103 (4) (2015) 1424–1435.
[16] K. Radad, M. Al-Shraim, R. Moldzio, W.D. Rausch, Recent advances in benefits and hazards of engineered nanoparticles, Environ. Toxicol. Pharmacol. 34 (3) (2012) 661–672.
[17] H.M. Saleh, A.I. Hassan, Synthesis and characterization of nanomaterials for application in cost-effective electrochemical devices, Sustainability 15 (14) (2023) 10891.
[18] S. Sagadevan, R. Schirhagl, M.Z. Rahman, M.F.B. Ismail, J.A. Lett, I. Fatimah, N.H.M. Kaus, W.C. Oh, Recent advancements in polymer matrix nanocomposites for bone tissue engineering applications, J. Drug Delivery Sci. Technol. (2023) 104313.
[19] S. Krishnamoorthy, N.N. Zait, A.M. Nasir, S.M. Ishar, N.H. Hamzah, R.D.R. Din, K. Osman, Towards development of green nanoparticles in applied health application: A mini review, Mater. Today: Proc. (2023) 1–9.

[20] N.A. Ismail, K.A.M. Amin, M.H. Razali, October. Preparation of gellan gum (GG) film: the effect of GG, calcium chloride ($CaCl_2$), glycerol concentration and heat treatment, IOP Conf. Ser.: Mater. Sci. Eng. 440 (2018) 012006.
[21] ASTM Subcommittee D20.10 on Mechanical Properties, Standard Test Method for Tensile Properties of Thin Plastic Sheeting, American Society for Testing and Materials, 1995.
[22] T. Kokubo, H. Takadama, How useful is SBF in predicting in vivo bone bioactivity?, Biomaterials 27 (15) (2006) 2907–2915
[23] K. Meera, M.T. Ramesan, Development of high-performance biopolymer nanocomposites derived from carboxymethyl chitosan/boehmite via green synthesis, Polym. Compos. 44 (2) (2023) 1135–1148.
[24] P.S. Gils, D. Ray, P.K. Sahoo, Designing of silver nanoparticles in gum arabic based semi-IPN hydrogel, Int. J. Biol. Macromol. 46 (2) (2010) 237–244.
[25] B. Singh, V. Sharma, H. Sen, Fabrication of acacia gum grafted copolymeric network hydrogel for biomedical applications, Bioact. Carbohydr. Diet. Fibre 29 (2023) 100353.
[26] H. Espinosa-Andrews, O. Sandoval-Castilla, H. Vázquez-Torres, E.J. Vernon-Carter, C. Lobato-Calleros, Determination of the gum Arabic–chitosan interactions by Fourier Transform Infrared Spectroscopy and characterization of the microstructure and rheological features of their coacervates, Carbohydr. Polym. 79 (3) (2010) 541–546.
[27] R.M. Daoub, A.H. Elmubarak, M. Misran, E.A. Hassan, M.E. Osman, Characterization and functional properties of some natural Acacia gums, J. Saudi Soc. Agric. Sci. 17 (3) (2018) 241–249.
[28] M.H. Razali, N.A. Ismail, K.A.M. Amin, Titanium dioxide nanotubes incorporated gellan gum bio-nanocomposite film for wound healing: Effect of TiO_2 nanotubes concentration, Int. J. Biol. Macromol. 153 (2020) 1117–1135.
[29] J. Hu, D. Li, Q. Huai, M. Geng, Z. Sun, M. Wang, S. Wang, Y. Li, H. Zheng, Development and evaluation of soybean protein isolate–based antibacterial nanocomposite films containing nano-TiO_2, Ind. Crop. Prod. 197 (2023) 116620.
[30] A.M. Adel, M.T. Al-Shemy, M.A. Diab, M. El-Sakhawy, R.G. Toro, L. Cerri, D. Caschera, Immobilization of TiO_2NP@ oxidized cellulose nanocrystals for paper-based active packaging materials, Int. J. Biol. Macromol. 231 (2023) 123270.
[31] N.A. Ismail, K.A.M. Amin, F.A.A. Majid, M.H. Razali, Gellan gum incorporating titanium dioxide nanoparticles biofilm as wound dressing: Physicochemical, mechanical, antibacterial properties and wound healing studies, Mater. Sci. Eng. C 103 (2019) 109770.
[32] S. Swain, T.Y. Kwon, T.R. Rautray, Fabrication of silver doped nano hydroxyapatite-carrageenan hydrogels for articular cartilage applications, bioRxiv (2021) 2020–2035.
[33] M.A. Masuelli, Hydrodynamic properties of whole arabic gum, Am. J. Food Sci. Tech. 1 (3) (2013) 60–66.
[34] B. Maharjan, D. Kumar, G.P. Awasthi, D.P. Bhattarai, J.Y. Kim, C.H. Park, C.S. Kim, Synthesis and characterization of gold/silica hybrid nanoparticles incorporated gelatin methacrylate conductive hydrogels for H9C2 cardiac cell compatibility study, Compos. B Eng. 177 (2019) 107415.
[35] E. Genskowsky, L.A. Puente, J.A. Pérez-Álvarez, J. Fernandez-Lopez, L.A. Muñoz, M. Viuda-Martos, Assessment of antibacterial and antioxidant properties of chitosan edible films incorporated with maqui berry (Aristotelia chilensis), LWT-Food Sci. Technol. 64 (2) (2015) 1057–1062.
[36] M. Haghi, M. Hekmatafshar, M.B. Janipour, S.S. Gholizadeh, M.K. Faraz, F. Sayyadifar, M. Ghaedi, Antibacterial effect of TiO_2 nanoparticles on pathogenic strain of *E. coli*, Int. J. Adv. Biotechnol. Res. 3 (3) (2012) 621–624.
[37] L. Cao, X. Wu, Q. Wang, J. Wang, Biocompatible nanocomposite of TiO_2 incorporated bi-polymer for articular cartilage tissue regeneration: a facile material, J. Photochem. Photobiol. B Biol. 178 (2018) 440–446.
[38] S. Tang, Z. Wang, P. Li, W. Li, C. Li, Y. Wang, P.K. Chu, Degradable and photocatalytic antibacterial Au-TiO_2/sodium alginate nanocomposite films for active food packaging, Nanomaterials 8 (11) (2018) 930.
[39] E. Abdolmajid, H. Kharazi, M. Chalaki, M. Khojasteh, S. Haghighat, F. Attar, F. Nemati, M. Falahati, Titanium oxide nanoparticles fabrication, hemoglobin interaction, white blood cells cytotoxicity, and antibacterial studies, J. Biomol. Struct. Dyn. 37 (11) (2019) 3007–3017.
[40] M.A. Vargas, J.E. Rodríguez-Páez, Facile synthesis of TiO_2 nanoparticles of different crystalline phases and evaluation of their antibacterial effect under dark conditions against *E. coli*, J. Clust. Sci. 30 (2019) 379–391.
[41] S. Dutta, T. Kar, D. Mandal, P.K. Das, Structure and properties of cholesterol-based hydrogelators with varying hydrophilic terminals: biocompatibility and development of antibacterial soft nanocomposites, Langmuir 29 (1) (2013) 316–327.
[42] R. Pandiyan, S. Ayyaru, Y.H. Ahn, Non-toxic properties of TiO_2 and $STiO_2$ nanocomposite PES ultrafiltration membranes for application in membrane-based environmental biotechnology, Ecotoxicol. Environ. Saf. 158 (2018) 248–255.
[43] S. Koch, M. Kessler, K. Mandel, S. Dembski, K. Heuzé, S. Hackenberg, Polycarboxylate ethers: The key towards non-toxic TiO_2 nanoparticle stabilisation in physiological solutions, Colloids Surf. B Biointerfaces 143 (2016) 7–14.
[44] F. Li, Y. Jiang, M. Chen, B. Yu, J. Wang, F. Wang, Effect of ZrO_2 addition on in-vitro bioactivity and mechanical properties of SiO_2–Na_2O–CaO–P_2O_5 bioactive glass-ceramic, Ceram. Int. 48 (13) (2022) 18541–18550.
[45] M.R. Filgueiras, G. La Torre, L.L. Hench, Solution effects on the surface reactions of a bioactive glass, J. Biomed. Mater. Res. 27 (4) (1993) 445–453.
[46] H. Gheisari, E. Karamian, M. Abdellahi, A novel hydroxyapatite–Hardystonite nanocomposite ceramic, Ceram. Int. 41 (4) (2015) 5967–5975.
[47] A. Ślósarczyk, Z. Paszkiewicz, C. Paluszkiewicz, FTIR and XRD evaluation of carbonated hydroxyapatite powders synthesized by wet methods, J. Mol. Struct. 744 (2005) 657–661.
[48] K.V. Kumar, T.J. Subha, K.G. Ahila, B. Ravindran, S.W. Chang, A.H. Mahmoud, O.B. Mohammed, M.A. Rathi, Spectral characterization of hydroxyapatite extracted from Black Sumatra and Fighting cock bone samples: A comparative analysis, Saudi J. Biol. Sci. 28 (1) (2021) 840–846.
[49] P. Surya, A. Nithin, A. Sundaramanickam, M. Sathish, Synthesis and characterization of nano-hydroxyapatite from Sardinella longiceps fish bone and its effects on human osteoblast bone cells, J. Mech. Behav. Biomed. Mater. 119 (2021) 104501.
[50] S.I. Jariya, N. Manivannan, B.M. Ali, T.S. Narayanan, K. Ravichandran, Engineering the surface of titanium to improve its bioactivity and antibacterial activity through a multi-functional coating approach, New J. Chem. 47 (12) (2023) 5843–5862.
[51] S.C. Wu, H.C. Hsu, H.C. Yu, C.E. Shen, W.F. Ho, Preparation and evaluation of osteoinductive porous biphasic calcium phosphate granules obtained from eggshell for bone tissue engineering, Adv. Powder Technol. 34 (1) (2023) 103909.
[52] L.C. Gerhardt, G.M.R. Jell, A.R. Boccaccini, Titanium dioxide (TiO_2) nanoparticles filled poly (D, L lactid acid) (PDLLA) matrix composites for bone tissue engineering, J. Mater. Sci. – Mater. Med. 18 (2007) 1287–1298.
[53] F.H. Haghighi, M. Mercurio, S. Cerra, T.A. Salamone, R. Bianymotlagh, C. Palocci, V.R. Spica, I. Fratoddi, Surface modification of TiO_2 nanoparticles with organic molecules and their biological applications, J. Mater. Chem. B 11 (2023) 2334–2366.